Complex band structure of topologically protected edge states

Xiaoqian Dang,[1] J. D. Burton,[1,*] Alan Kalitsov,[2] Julian P. Velev,[1,2] and Evgeny Y. Tsymbal[1,†]

[1]*Department of Physics and Astronomy & Nebraska Center for Materials and Nanoscience, University of Nebraska, Lincoln, Nebraska 68588-0299, USA*

[2]*Department of Physics and Astronomy and Institute for Functional Nanomaterials, University of Puerto Rico, San Juan, Puerto Rico 00931, USA*

(Received 5 September 2014; revised manuscript received 22 September 2014; published 14 October 2014)

One of the great successes of modern condensed matter physics is the discovery of topological insulators (TIs). A thorough investigation of their properties could bring such materials from fundamental research to potential applications. Here, we report on theoretical investigations of the complex band structure (CBS) of two-dimensional (2D) TIs. We utilize the tight-binding form of the Bernevig, Hughes, and Zhang model as a prototype for a generic 2D TI. Based on this model, we outline the conditions that the CBS must satisfy in order to guarantee the presence of topologically protected edge states. Furthermore, we use the Green's function technique to show how these edge states are localized, highlighting the fact that the decay of the edge-state wave functions into the bulk of a TI is not necessarily monotonic and, in fact, can exhibit an oscillatory behavior that is consistent with the predicted CBS of the bulk TI. These results may have implications for electronic and spin transport across a TI when it is used as a tunnel barrier.

DOI: 10.1103/PhysRevB.90.155307 PACS number(s): 73.43.−f, 85.75.−d, 72.25.Mk, 73.20.−r

I. INTRODUCTION

Arguably one of the most exciting recent developments in condensed matter physics is the discovery of topological insulators (TIs) [1]. Traditionally, different states of matter are classified according to the symmetries that are spontaneously broken. The quantum Hall effect, which is the quantization of the conductance of two-dimensional (2D) electron gas in a magnetic field, is the first example of a topological state, a different state of matter that does not break any symmetry [2]. This state is characterized by a topological constant, a Chern number, independent of the geometry [3]. More recently, a quantum spin Hall effect (QSH) has been predicted, which is a quantization of the conductance produced intrinsically by the spin-orbit interaction and does not require any applied magnetic field [4]. The QSH state is characterized by a bulk band gap, hence, a topological insulator and gapless surface states. Unlike the quantum Hall state, the QSH state preserves time-reversal symmetry, and consequently, charges with opposite spins move in the opposite direction, resulting in net spin transport (for a recent review, see Ref. [5]). The QSH state is characterized by a nonzero topological constant Z_2, analogous to a Chern number for time-reversal-invariant systems [4], which distinguishes it from the ordinary band insulator. At the interface of a TI with a band insulator (or vacuum), the Z_2 quantum number is not conserved, necessitating the appearance of a conducting surface state.

As it is a relativistic effect, the spin-orbit interaction is large in heavy elements; therefore, the QSH state was proposed to exist, and shortly after, observed in HgTe/CdTe quantum wells [6,7]. The physics of the QSH state is based on the inverted band structure, where the valence and conduction bands of different parity cross, and a band gap is opened due to the spin-orbit interaction. The change of the valence band parity is associated with a change in the topological constant Z_2 [8]. Based on this observation, a tight-binding model for 2D TIs was developed by Bernevig, Hughes, and Zhang (BHZ) [6]. This model represents a low-energy Taylor expansion of the Hamiltonian of the system truncated to only the lowest conduction and the highest valence bands. It has been shown to map on to a three-dimensional TI model in the limit of a thin film [9]. The model can also be formulated in real space, which is more suitable for modeling finite systems involving surfaces or interfaces [8].

Shortly after the experimental confirmation of the QSH state in two dimensions, three-dimensional TIs have been discovered in the Bi_2Se_3 family of materials [10–12]. Subsequently, a concerted effort has been directed towards the discovery of new TIs [13]. As a result many other compounds have been predicted to be TIs, including complex oxides, such as Na_2IrO_3 [14] and Sr_2IrO_4 [15], which exhibit strong onsite Coulomb repulsion and large band gaps. The direct way to determine if a compound is a TI is to calculate the Z_2 quantum number from the band structure [4], which is similar to a Berry phase calculation [16]. In compounds with inversion symmetry, however, a much simpler criterion has been devised based on examining the parity of the valence bands [8].

A new insight into the properties of TIs can be obtained by looking at their complex band structure (CBS). Complex band structure is an analytic continuation of the real band structure into the complex momentum space [17]. In the energy band regions, complex solutions for the band structure represent evanescent states rather than propagating Bloch states of a crystal. This approach has been efficiently used in the field of spin-polarized tunneling [18], where the CBS of the tunneling barrier material was found to have profound implications for tunneling magnetoresistance through symmetry filtering of the propagating states [19,20] and for spin filtering through the spin-dependent decay rate of the evanescent states [21]. In the case of TIs, the bulk evanescent states are expected to be intrinsically coupled to the topologically protected states. Furthermore, the topologically nontrivial band structure of the

*jdburton1@gmail.com
†tsymbal@unl.edu

TIs may provide novel opportunities for nonconventional spin filtering when TIs are used as tunnel barriers.

In this paper, we explore in some detail the CBS of 2D TIs. We utilize the real-space formulation of the BHZ model and lay out the basic requirements for the CBS that give rise to the localized topologically protected edge states. Furthermore, we use the Green's function formalism to study the decay of the edge states into the bulk of the TI and elucidate the predicted behavior in terms of the CBS.

II. METHODOLOGY

A. Real-space parameterization

We use the real-space formulation [8] of the BHZ tight-binding model [6]. The model consists of a 2D square lattice (lattice constant a), where each site hosts three p orbitals and one s orbital for each spin. As shown in Fig. 1(a), it is assumed that in the barycenter potential (i.e., spherically averaged) the s states lie lower than the p states. The crystal field of the square lattice breaks the degenerate p orbitals into low lying out-of-plane p_z orbitals and higher energy in-plane (p_x, p_y) orbitals. The spin-orbit interaction splits the in-plane orbitals (with total angular momentum $j = 3/2$) into a lower doublet with $|m_j| = 3/2$ and a higher doublet with $|m_j| = 1/2$. Finally, the states couple from site-to-site leading to bands which, in the absence of s-p coupling, would overlap around the Fermi level (E_F). It is this overlap and s-p coupling that gives rise to the bulk band-gap and topologically protected edge states. The Hamiltonian can be written in a basis that includes four physically important states closest to the Fermi level: $|s_{1/2,\pm 1/2}\rangle = |s, \pm\frac{1}{2}\rangle$ and $|p_{3/2,\pm 3/2}\rangle = |p_x \pm i\,p_y, \pm\frac{1}{2}\rangle$.

Matrix elements of the Hamiltonian are written in terms of four parameters: the onsite energy of s and p states ε_s and ε_p, respectively, and three (positive) integrals t_{ss}, t_{pp}, and t_{sp} for hopping between s orbitals, p orbitals, and intersite s-p hybridization, respectively. Since the spin-orbit interaction is implicitly included in the construction of the basis, the Hamiltonian is block-diagonal in spin-space with a simple relationship between the two spin blocks, as described in the following.

The Hamiltonian matrix elements for intersite s-p coupling contain important phase factors that depend on the direction of hopping [8], as shown in Fig. 1(b). The spin-up sector of the Hamiltonian itself consists of the 2×2 block matrices

$$H^{\uparrow}_{0,0} = \begin{pmatrix} \varepsilon_s & 0 \\ 0 & \varepsilon_p \end{pmatrix},$$
$$H^{\uparrow}_{1,0} = \begin{pmatrix} t_{ss} & t_{sp} \\ -t_{sp} & -t_{pp} \end{pmatrix}, \quad H^{\uparrow}_{0,1} = \begin{pmatrix} t_{ss} & it_{sp} \\ it_{sp} & -t_{pp} \end{pmatrix}, \tag{1}$$

which describe the onsite and nearest-neighbor hopping along the positive x and y directions, respectively. The blocks describing hopping in opposite directions are related by Hermitian conjugation: $H_{-1,0} = H^{\dagger}_{1,0}$ and $H_{0,-1} = H^{\dagger}_{0,1}$. It is straightforward to show that, since the up- and down-spin basis states differ only in the sign of the p_y component, the blocks describing the spin-down sector are equal to the transpose of those in Eq. (1). Throughout the remainder of this paper, we focus on the spin-up sector of the Hamiltonian and drop the explicit reference to the spin.

In the bulk, i.e., an infinite 2D lattice, the eigenstates can be found using the Bloch ansatz, $\psi(n,m) = \exp(ik_x na + ik_y ma)\mathbf{u}$, where n and m are site indices along the x and y directions, respectively. The two component vector $\mathbf{u}$ is an eigenvector of the Bloch Hamiltonian

$$H(\mathbf{k}) = H_{0,0} + H_{1,0}e^{ik_x a} + H_{-1,0}e^{-ik_x a} + H_{0,1}e^{ik_y a} + H_{0,-1}e^{-ik_y a} \tag{2}$$

with eigenvalue $E(\mathbf{k})$. Here, $\mathbf{k} = (k_x, k_y)$ is a wave vector in the 2D Brillouin zone with purely real components; therefore, bulk states are delocalized throughout the entire crystal. To study topologically protected edge states, however, such solutions alone are insufficient because they cannot describe localized states in the band gap. Therefore, we appeal to the techniques described in the next two subsections.

B. Complex band structure

Electronic states within the bulk band gap can be described by extending the search for eigenstates with the complex wave vector. For example, if we consider a semi-infinite half space having sites only for $n \geqslant 0$, with a straight edge along the y direction, then periodicity along the x direction is removed. We, therefore, use an ansatz $\psi(n,m) = \lambda^n \exp(ik_y ma)\mathbf{u}$, where λ is

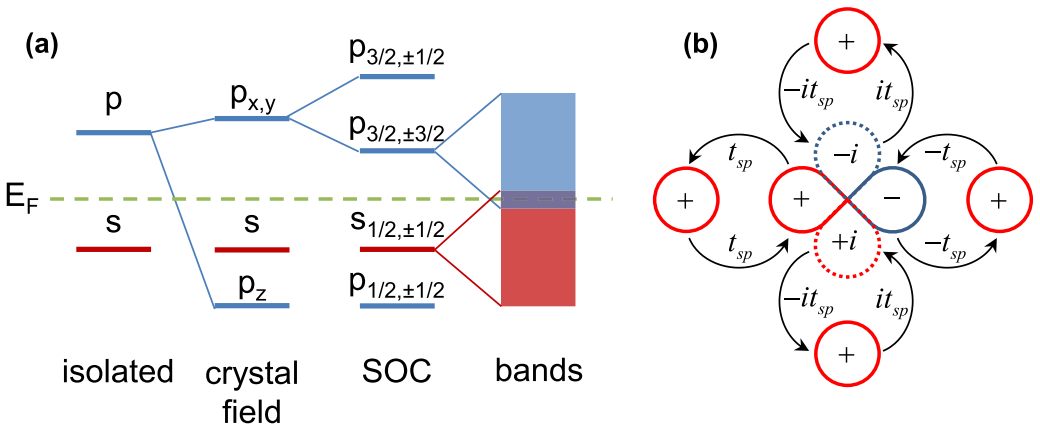

FIG. 1. (Color online) (a) Energy-level diagram of the model. (b) Schematic demonstrating the phase factors appearing in the intersite s-p hopping elements in Eq. (1) for the spin-up channel. Circles represent s orbital basis states on sites neighboring the central p orbital.

a generalization of the Bloch phase factor allowing for complex values of k_x, i.e., $\lambda = \exp(ik_x a)$. Such states can be used to describe a system with nonperiodic boundary conditions, such as topologically protected edge states, because they are exponentially localized, decaying toward $n = -\infty$ for $|\lambda| > 1$ and toward $n = +\infty$ for $|\lambda| < 1$. In contrast to bulk states, where the general procedure is to first pick a real $\mathbf{k}$ in the 2D Brillouin zone and find the energy, the approach here is reversed. For a fixed energy E (e.g., within the bulk band gap), the ansatz given previously yields the following equation for λ and the eigenvector $\mathbf{u}$:

$$[\tilde{H}_0(k_y) - E + \tilde{H}_1\lambda + \tilde{H}_{-1}\lambda^{-1}]\mathbf{u} = \mathbf{0}, \tag{3}$$

where $\tilde{H}_1 = H_{1,0}, \tilde{H}_{-1} = H_{-1,0}$, and

$$\tilde{H}_0(k_y) = H_{0,0} + H_{0,1}e^{ik_y a} + H_{0,-1}e^{-ik_y a} \tag{4}$$

is the Hamiltonian of an isolated infinite chain of sites along the y direction. Equation (3) is a nonlinear eigenvalue problem that can be rewritten as a linear generalized eigenvalue problem of double the size and can be solved numerically in a straightforward fashion [22,23]. The corresponding spectrum of complex energy-dependent k_x values is known collectively as the CBS. Note that the CBS is inherently a bulk property, being derived from the same parameters that describe the bulk. In fact, states with $|\lambda| = 1$ correspond precisely to the bulk band structure, which is described by the extended Bloch states. The remaining states with $|\lambda| \neq 1$ decay/grow exponentially in space and, therefore, cannot be made to match the periodic boundary conditions of the bulk, but instead, describe localized states. All states in the CBS, localized or extended, must be included when finding solutions that match boundary conditions of finite or semi-infinite geometries [24].

Three possible types of solutions of Eq. (3) for λ have (i) purely real k_x, corresponding to bulklike states, (ii) purely imaginary k_x, corresponding to states that decay/grow monotonically along the x direction, and (iii) complex k_x, which decay/grow exponentially at a rate $\mathrm{Im}(k_x)$ and oscillate with wave vector $\mathrm{Re}(k_x)$.

For every given energy E and k_y, there are, in our 2×2 basis, four solutions to Eq. (3). A subset of the solutions with $|\lambda| \neq 1$ form the basis of the topologically protected edge states, which may or may not be present within the bulk band gap. Here, we show analytically the conditions for such states to exist and their relationship to the CBS.

A general property of the CBS for any system with inversion symmetry is that if, say, λ_1 is a solution, then $1/\lambda_1$ is also a solution. Of the four solutions of Eq. (3), therefore, there are two solutions with $|\lambda| < 1$, which decay into the positive x direction. These two eigenstates, which we label as λ_1 and λ_2 with corresponding eigenvectors $\mathbf{u}_1$ and $\mathbf{u}_2$, must form any edge state that might exist

$$\psi(n) = \lambda_1^n \mathbf{u}_1 + r\lambda_2^n \mathbf{u}_2, \tag{5}$$

where r is a coefficient chosen to satisfy the boundary conditions at the edge, namely, $\psi(-1) = \mathbf{0}$. It is straightforward to see that for a nontrivial state to exist, $\mathbf{u}_1$ and $\mathbf{u}_2$ can differ by, at most, a constant of proportionality. Thus, the edge state must have the form

$$\psi(n) = \left(\lambda_1^n + r\lambda_2^n\right)\mathbf{u}, \tag{6}$$

where $r = -\lambda_2/\lambda_1$ satisfies the edge boundary condition.

Thus, we find that for an edge state to exist with energy E and wave vector k_y the CBS must contain two states that

(i) have different values of λ,
(ii) both satisfy $|\lambda| < 1$,
(iii) share a common eigenvector $\mathbf{u}$.

Criterion (i) follows from the fact that if $\lambda_1 = \lambda_2$, then the state in Eq. (6) is trivial. If there are states in the CBS that satisfy these conditions, then it is straightforward to use Eq. (3) to find the allowed eigenvectors. Since both λ_1 and λ_2 must solve Eq. (3) at the same E and k_y we find that $\mathbf{u}$ must satisfy

$$(\lambda_1 - \lambda_2)\tilde{H}_1\mathbf{u} + \left(\lambda_1^{-1} - \lambda_2^{-1}\right)\tilde{H}_{-1}\mathbf{u} = \mathbf{0}. \tag{7}$$

Equation (7) is a simple generalized eigenvalue problem, with $\mathbf{u}$ being an eigenvector. Solving Eq. (7), the allowed (unnormalized) eigenvectors for edge states in our system are

$$\mathbf{u}_\pm = \begin{pmatrix} \sqrt{t_{pp}} \\ \pm\sqrt{t_{ss}} \end{pmatrix}. \tag{8}$$

Substituting Eq. (8) into Eq. (3), we can immediately find solutions for E and λ. The dispersion relationships for the edge states corresponding to $\mathbf{u}_\pm$ are

$$E_\pm(k_y) = \mp\frac{4t_{sp}\sqrt{t_{ss}t_{pp}}\sin(k_y a)}{t_{ss} + t_{pp}} + \frac{\varepsilon_s t_{pp} + \varepsilon_p t_{ss}}{t_{ss} + t_{pp}}. \tag{9}$$

Here, we see that whenever the conditions set out above are satisfied, edge states appear in the gap that have a linear dispersion around $k_y = 0$. The center of the edge band is at a weighted average energy, with weights determined by the intraband hopping integrals t_{ss} and t_{pp}.

The expressions for the corresponding four values of λ are too cumbersome to reproduce here. Conditional analysis of λ at $k_y = 0$, however, against criteria (i)–(iii) presented previously, reveal that edge states exist only when

$$\varepsilon_p - \varepsilon_s \leqslant 4(t_{ss} + t_{pp}), \tag{10}$$

with the system being a simple band insulator otherwise. Simply put, Eq. (10) is the requirement that the s-like band and the p-like band must overlap; therefore, due to the t_{sp} coupling, a topologically nontrivial band gap opens. This condition is precisely the same as that arrived at by Fu and Kane [8] through symmetry analysis of the BHZ model. In Sec. III, we present results with definite model parameters to demonstrate this topological condition.

C. Surface Green's function

The Green's function method as applied to tight-binding systems is a powerful approach to exploring the electronic structure of real-space systems, such as edges. The key feature of the approach is the application of the Dyson equation, which relates perturbations to the Hamiltonian to changes in the Green's function in a straightforward fashion.

We consider the system shown in Fig. 2 consisting of an isolated, infinite chain of lattice sites at $n = 0$, oriented along

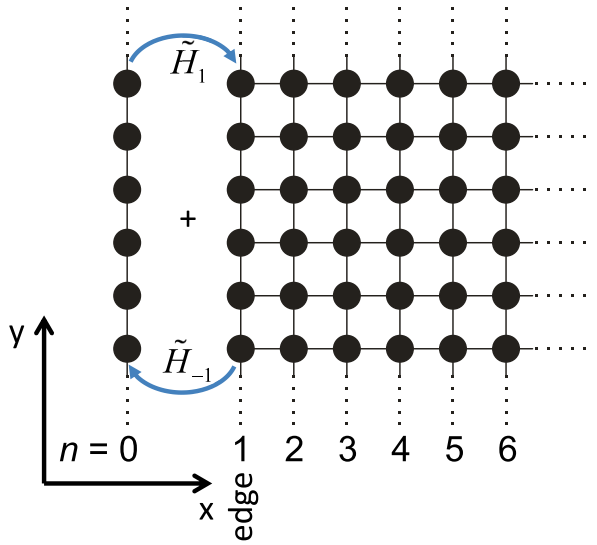

FIG. 2. (Color online) Schematic geometry of the edge showing the construction of the Dyson equation. The unperturbed system, described by Green's function g, consists of an isolated, infinite chain of lattice sites along the y direction and a semi-infinite half plane. Introduction of coupling between the chain and the edge leads to the perturbed system, a lone semi-infinite half plane with $n>0$, described by the Green's function G.

the y direction, described by $\tilde{H}_0(k_y)$, given in Eq. (4). In addition to this chain is a semi-infinite half plane of sites with $n \geqslant 1$, which can be considered as a set of identical parallel chains, each of which is coupled to its nearest neighbors by $\tilde{H}_1$ and $\tilde{H}_{-1}$. The Green's function for this system is $g_{nn'}$, a 2×2 matrix describing the propagation from chain n to chain n' along the x direction. Propagation along the y direction is simple owing to the periodic boundary conditions; therefore, the Green's function is diagonal in k_y. It is clear that $g_{0n} = g_{n0} = 0$ for all $n > 0$, since there is no coupling between the chain and the edge; therefore, g_{00} is straightforward to calculate

$$g_{00}(E,k_y) = [E + i\eta - \tilde{H}_0(k_y)]^{-1}, \tag{11}$$

where $\eta > 0$ is an infinitesimal energy introduced to broaden the band structure of $\tilde{H}_0(k_y)$. In the numerical results presented in Sec. III a small but finite η is used to resolve narrow energy levels.

Next, we introduce coupling between the chain at $n = 0$ and the edge at $n = 1$. The Dyson equation relates the Green's function of the coupled system $G_{nn'}$ to that of the uncoupled system, $g_{nn'}$. Using the fact that the coupled system is identical to the semi-infinite part of the uncoupled system, i.e., $G_{00} = g_{11}$, we find

$$G_{00} = g_{00} + g_{00}\tilde{H}_1 G_{00}\tilde{H}_{-1}G_{00}. \tag{12}$$

Equation (12) is a quadratic matrix equation for G_{00}. A number of well-established, numerically exact procedures exist to find the solution of such an equation [23,25]. The power of the real-space Green's function technique is that once G_{00} is calculated, all other elements $G_{nn'}$ can be found through recursion of the Dyson equation. In particular, the onsite elements of the Green's function obey a straightforward recursive relationship between layer n and layer $n + 1$:

$$G_{n+1,n+1} = G_{00} + G_{00}\tilde{H}_1 G_{nn}\tilde{H}_{-1}G_{00}. \tag{13}$$

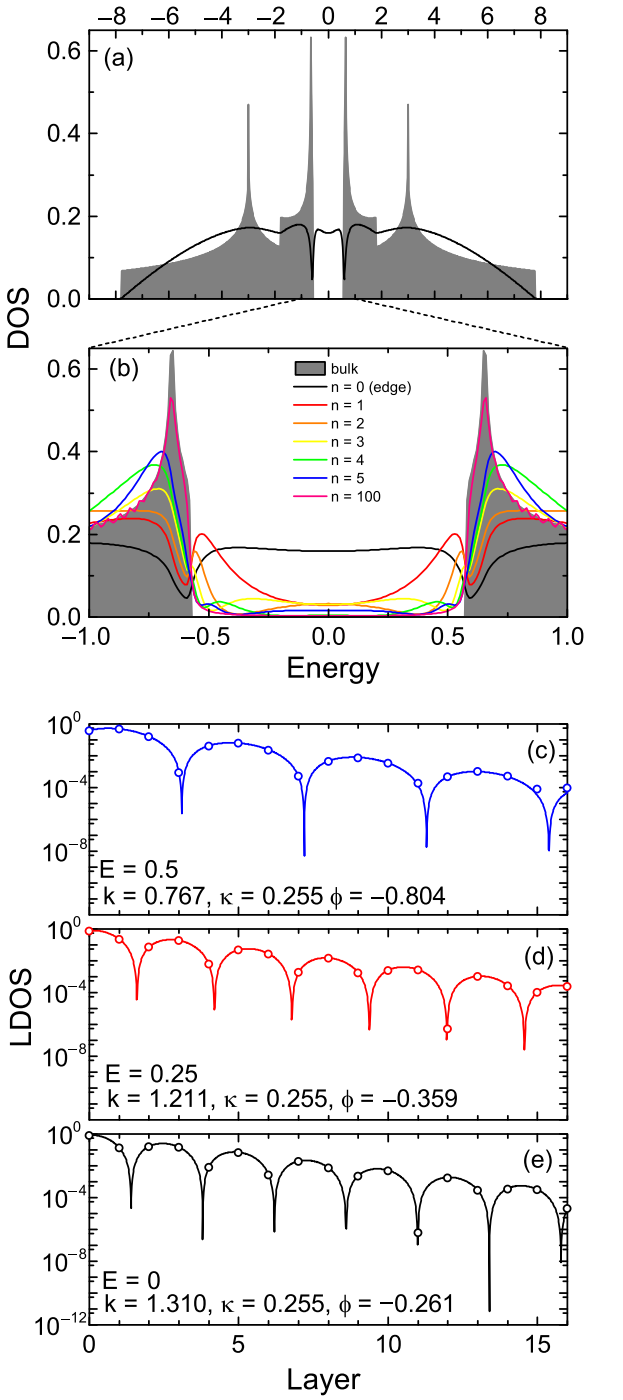

FIG. 3. (Color online) The layer-resolved LDOS near the edge of the model TI (a) over the entire range of bands and (b) in the region of the bulk band gap. Model parameters are $a = 1$, $t = 1.2$, $t_{sp} = 0.3$, and $\varepsilon = 3.0$. The total DOS in the bulk (filled curves) was integrated using a uniform 500×500 **k**-mesh. The LDOS for layers near the edge is computed using Eq. (14), with an energy broadening of $\eta = 0.01$ and integrated using a mesh of 500 k_y points. (c)–(e) Layer dependence of the LDOS at $E = 0.50$, 0.25, and 0, respectively. Curves are calculated using Eq. (19), with parameters derived from the CBS given in the figures.

Using Eq. (13), we can find the k_y-resolved local density of states (LDOS) on any layer n

$$\rho_n(E,k_y) = -\frac{1}{\pi}\mathrm{Tr}[\mathrm{Im}G_{nn}(E,k_y)], \tag{14}$$

where Tr is the trace over the orbital indices. The total LDOS for a given layer is obtained by integrating over the one-dimensional Brillouin zone. In Sec. III we use the LDOS to show the existence (or absence) of the topologically protected edge states with definite model parameter, along with how the CBS determines their localization at the edge.

III. RESULTS AND DISCUSSION

A. LDOS near the edge

We begin by reducing the number of model parameters by assuming a system with electron-hole symmetry, i.e., $\varepsilon_p = -\varepsilon_s = \varepsilon > 0$ and $t_{ss} = t_{pp} = t > 0$. In Figs. 3(a) and 3(b), we plot the layer-resolved integrated LDOS, computed using the Green's function techniques outlined in Sec. II C . Model parameters given in the figure caption satisfy the condition in Eq. (10), ensuring the presence of edge states. The total density of states (DOS) in the bulk is computed using the triangle method [26] to sample the 2D Brillouin zone. We clearly see from Fig. 3(a) that while a gap exists in the bulk DOS, near the edge, there are states within the gap. In Fig. 3(b), we see that these gap states decay away from the edge in a nontrivial manner. For example, around $E = 0.25$, the $n = 3$ layer has larger density than for $n = 2$. This oscillatory decay is clearly seen in Figs. 3(c)–3(e), where data points are the calculated LDOS on different layers at specific energies.

For more detail, Fig. 4 shows the k_y-resolved LDOS in the energy range around the bulk band-gap for several layers near the interface. In each layer, there are clear signatures of the conduction and valence bands, similar to what is seen in the bulk. Within the band-gap, however, a one-dimensional band is present whose density decays in magnitude from the edge into the bulk. The decay of this edge state, however, is not uniform in real space (i.e., it oscillates along with the decay) nor is this oscillation uniform in energy (i.e., the spatial oscillation is not the same for all energies). We note that the density oscillations, seen in Fig. 4 in the bulklike conduction and valence bands for the layers near the edge, are due to interference of the incident and reflected Bloch waves in the continuum energy spectrum and are unrelated to the topology of the band structure.

B. CBS of the edge states

For our model electron-hole symmetry, we follow the procedure given in Sec. II A and find that the edge states, should they exist, are described by the (normalized) eigenvectors and corresponding dispersion relations

$$\mathbf{u}_\pm = \frac{1}{\sqrt{2}}\begin{pmatrix}1\\ \pm 1\end{pmatrix}, \quad E_\pm(k_y) = \mp 2t_{sp}\sin(k_y a). \tag{15}$$

The generalized Bloch factors are given by

$$\lambda_+^\pm = -\frac{1}{2}\frac{E_0(k_y) \pm \sqrt{E_0(k_y)^2 - 4\left(t^2 - t_{sp}^2\right)}}{t + t_{sp}} \tag{16}$$

$$\lambda_-^\pm = -\frac{1}{2}\frac{E_0(k_y) \pm \sqrt{E_0(k_y)^2 - 4\left(t^2 - t_{sp}^2\right)}}{t - t_{sp}}, \tag{17}$$

where

$$E_0(k_y) = 2t\cos(k_y a) - \varepsilon. \tag{18}$$

If the system is to be a topological insulator, it must satisfy criteria (i)–(iii), given previously, at least at $k_y = 0$ and $E = 0$. In Figs. 5(a) and 5(b), we plot the complex k_x as a function of ε for $k_y = 0$ and $E = 0$, according to Eqs. (16) and (17). We see that for $\varepsilon < 4t$, both branches of Eq. (16) satisfy $\mathrm{Im}(k_x) > 0$; therefore, an edge state is expected. For $\varepsilon > 4t$, however, the two branches have different sign of $\mathrm{Im}(k_x)$ and therefore cannot form an edge state, thus making the system a simple band insulator. This can be seen by comparing Figs. 5(c) and 5(d), where for $\varepsilon = 2t$, we find an edge state in the k_y-resolved LDOS on the edge but not for $\varepsilon = 5t$. The critical value of $\varepsilon = 4t$ is also consistent with Eq. (10).

With the model parameters given in the caption of Fig. 3, solutions described by $\mathbf{u}_+$ and $\lambda_+^\pm$ meet criteria (i)–(iii), given in Sec. II A, for a range of k_y. Note that the narrow edge states shown in Fig. 4 match the negative sign of the dispersion relation predicted by Eq. (15) for the $\mathbf{u}_+$ states.

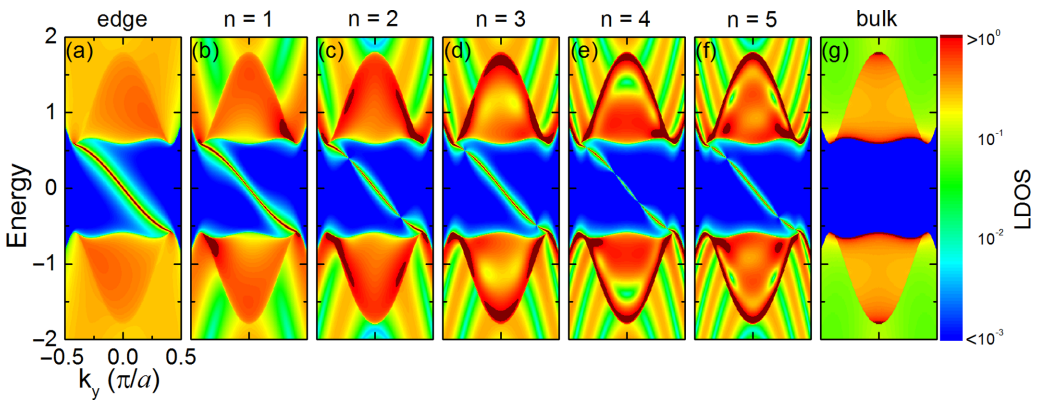

FIG. 4. (Color online) The k_y-resolved spin-up LDOS of the model topological insulator in the region around the bulk band gap for (a) the edge, (b)–(f) layers one through five, respectively, and (g) the bulk. Panels (a)–(f) use a broadening of $\eta = 0.01$ to resolve the δ-function-like gap states. The bulk DOS, (g), does not require broadening. The spin-down LDOS is the mirror image of each panel around $k_y = 0$. Model parameters are given in the caption of Fig. 3.

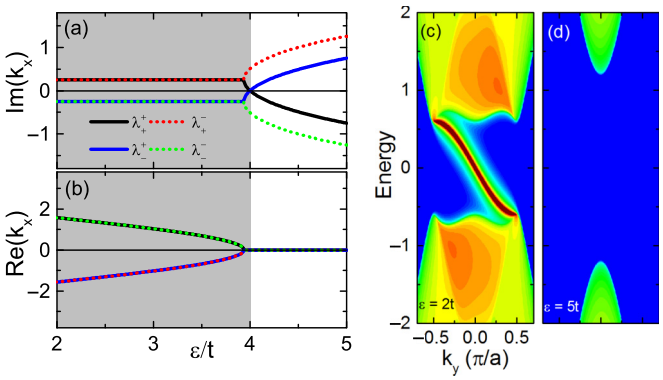

FIG. 5. (Color online) Dependence of the CBS and band topology on ε. (a) and (b) The imaginary and real parts of $k_x = -ia^{-1}\ln\lambda$ for the CBS state at $k_y = 0$ and $E = 0$. Solid and dotted curves correspond to $\mathbf{u}_+$ and $\mathbf{u}_-$ from Eq. (15), respectively. Criteria for a topologically nontrivial state are satisfied for $\varepsilon < 4t$, denoted by the filled background. (c) and (d) k_y-resolved LDOS at the edge for (c) $\varepsilon = 2t$ showing a topologically protected edge state and (d) $\varepsilon = 5t$ showing a simple band-insulating state. The color scale is the same as in Fig. 4. Parameters t and t_{sp} are fixed to the values given in the caption of Fig. 3.

The decay and oscillation of the edge states seen in Figs. 3 and 4 are a direct consequence of the CBS. In Fig. 6, we plot the real and imaginary parts of k_x corresponding to Eq. (16) as a function of k_y over the one-dimensional Brillouin zone using the model parameters specified in the caption of Fig. 3. First, we note that criterion (ii) for the formation of an edge

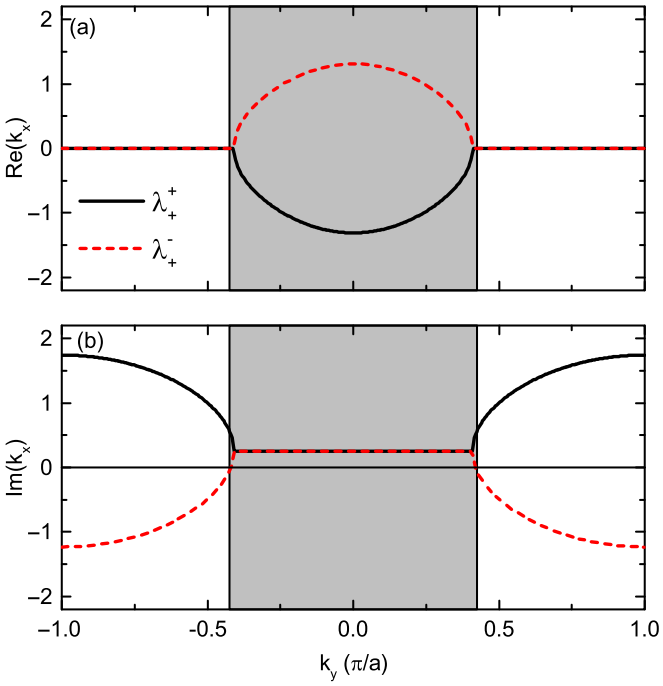

FIG. 6. (Color online) The complex bands for $\mathbf{u}_+$ described by Eq. (16). The real part of k_x is plotted in (a) and the corresponding imaginary part plotted in (b). Solid and dashed curves correspond to λ_+^+ and λ_+^-, respectively. The shaded region indicates the range over which the criteria for forming an edge state are satisfied. Model parameters are given in the caption of Fig. 3.

state are satisfied only over a range of k_y values, as marked by the shaded regions in Fig. 6. This matches what we have found from our analysis of the k_y-resolved LDOS plotted in Fig. 4, where it is clear that the gap states only exist over the same finite range of k_y. Second, we note that over most of the range of the edge states, there is indeed a nonzero value of $\mathrm{Re}(k_x)$ for both contributions; therefore, the LDOS is expected to have an oscillatory dependence. Also, over most of this range the exponential decay factor, governed by $\mathrm{Im}(k_x)$, is constant.

These properties are entirely consistent with the integrated LDOS shown in Fig. 3. The LDOS on layer n is given by $|\psi(n)|^2$, where $\psi(n)$ is defined by Eq. (6). The decay and oscillation of the LDOS is determined by the interference between the two waves in Eq. (6). As shown in Fig. 6, over most of the band gap, the decay parameter $\kappa = |\mathrm{Im}(k_x)|$ is the same for both components of the edge state, whereas the real components are equal in magnitude and opposite in sign, i.e., $k = \mathrm{Re}(k_x^+) = -\mathrm{Re}(k_x^-)$. The oscillation period of $|\psi|^2$ is determined by the difference in the real component of the contributing wave vectors [19] (which, in our case, is $2k$), and the LDOS follows a simple spatial dependence of the form

$$\mathrm{LDOS} \propto \cos^2(kx - \phi)\, e^{-2\kappa x}. \tag{19}$$

Using the parameters extracted from the CBS and treating ϕ as a fitting parameter, we plot Eq. (19) in Figs. 3(c)–3(e) along with the LDOS data from the Green's function analysis. Nearly perfect agreement is found. The small discrepancies for large energy and large layer index in Fig. 3(c) arise due to the broadening and finite sampling of k_y in the Green's function calculation.

IV. SUMMARY

By analyzing the required features of a topologically protected edge state, we have uncovered a different route to characterize topological insulators, namely, through their CBS. The requisite criteria are established and tested against the generic BHZ tight-binding model for a 2D TI. Further, the appearance and localization of the topologically protected edge states are described using a real space Green's function approach, which confirms the predictions made based on the CBS.

In addition to establishing these criteria, we found that, in general, the decay of the topologically protected edge state into the bulk of a topological insulator is not necessarily monotonic but, in fact, exhibits an oscillatory spatial dependence along with an exponential decay. The period of the oscillations, and the decay rate itself, is a direct consequence of the features of the CBS. These results may have implications for electronic and spin transport across a TI when it is used as a tunnel barrier.

ACKNOWLEDGMENTS

This research was supported by the National Science Foundation (NSF) under the Designing Materials to Revolutionize and Engineer our Future (DMREF) Program (Grant No. DMR-1234096) and the Nebraska Materials Research Science and Engineering Center (Grant No. DMR-0820521). The work at the University of Puerto Rico was supported by the NSF under the Experimental Program to Stimulate Competitive Research (Grants No. EPS-1002410 and No. EPS-1010094).

[1] J. E. Moore, Nature (London) **464**, 194 (2010).
[2] K. V. Klitzing, G. Dorda, and M. Pepper, Phys. Rev. Lett. **45**, 494 (1980).
[3] D. J. Thouless, M. Kohmoto, M. P. Nightingale, and M. den Nijs, Phys. Rev. Lett. **49**, 405 (1982).
[4] C. L. Kane and E. J. Mele, Phys. Rev. Lett. **95**, 226801 (2005).
[5] M. Z. Hasan and C. L. Kane, Rev. Mod. Phys. **82**, 3045 (2010).
[6] B. A. Bernevig, T. A. Hughes, and S. C. Zhang, Science **314**, 1757 (2006).
[7] M. König, S. Wiedmann, C. Brüne, A. Roth, H. Buhmann, L. W. Molenkamp, X. L. Qi, and S. C. Zhang, Science **318**, 766 (2007).
[8] L. Fu and C. L. Kane, Phys. Rev. B **76**, 045302 (2007).
[9] C.-X. Liu, H. J. Zhang, B. Yan, X.-L. Qi, T. Frauenheim, X. Dai, Z. Fang, and S.-C. Zhang, Phys. Rev. B **81**, 041307(R) (2010).
[10] D. Hsieh, D. Qian, L. Wray, Y. Xia, Y. S. Hor, R. J. Cava, and M. Z. Hasan, Nature (London) **452**, 970 (2008).
[11] H. Zhang, C. X. Liu, X. L. Qi, X. Dai, Z. Fang, and S.-C. Zhang, Nat. Phys. **5**, 438 (2009).
[12] D. Hsieh, Y. Xia, D. Qian, L. Wray, F. Meier, J. H. Dil, J. Osterwalder, L. Patthey, A. V. Fedorov, H. Lin, A. Bansil, D. Grauer, Y. S. Hor, R. J. Cava, and M. Z. Hasan, Phys. Rev. Lett. **103**, 146401 (2009).
[13] K. Yang, W. Setyawan, S. Wang, M. Buongiorno Nardelli, and S. Curtarolo, Nat. Mater. **11**, 614 (2012).
[14] C. H. Kim, H. S. Kim, H. Jeong, H. Jin, and J. Yu, Phys. Rev. Lett. **108**, 106401 (2012).
[15] J. M. Carter, V. V. Shankar, M. A. Zeb, and H. Y. Kee, Phys. Rev. B **85**, 115105 (2012).
[16] M. V. Berry, Proc. R. Soc. London. A **392**, 45 (1984)
[17] V. Heine, Proc. Phys. Soc. London **81**, 300 (1962); Phys. Rev. **138**, A1689 (1965).
[18] Ph. Mavropoulos, N. Papanikolaou, and P. H. Dederichs, Phys. Rev. Lett. **85**, 1088 (2000).
[19] W. H. Butler, X. G. Zhang, T. C. Schulthess and J. M. MacLaren, Phys. Rev. B **63**, 054416 (2001).
[20] J. P. Velev, K. D. Belashchenko, D. A. Stewart, M. van Schilfgaarde, S. S. Jaswal, and E. Y. Tsymbal, Phys. Rev. Lett. **95**, 216601 (2005); J. P. Velev, K. D. Belashchenko, S. S. Jaswal, and E. Y. Tsymbal, Appl. Phys. Lett. **90**, 072502 (2007).
[21] P. V. Lukashev, A. L. Wysocki, J. P. Velev, M. van Schilfgaarde, S. S. Jaswal, K. D. Belashchenko, and E. Y. Tsymbal, Phys. Rev. B **85**, 224414 (2012).
[22] Y. C. Chang and J. N. Schulman, Phys. Rev. B **25**, 3975 (1982).
[23] J. Velev and W. Butler, J. Phys.: Condens. Matter **16**, R637 (2004).
[24] P. S. Krstić, X.-G. Zhang, and W. H. Butler, Phys. Rev. B **66**, 205319 (2002).
[25] K. S. Dy, S. Y. Wu, and T. Spratlin, Phys. Rev. B **20**, 4237 (1979).
[26] J. H. Lee, T. Shishidou, and A. J. Freeman, Phys. Rev. B **66**, 233102 (2002).